J. Fluid Mech. (1989), *vol.* 201, *pp.* 203–221
Printed in Great Britain

Three-dimensional numerical simulation of flows past scoops in a gas centrifuge

By TAKUYA MATSUDA†, NAOKI TAMURA† AND KEISUKE SAWADA‡

† Department of Aeronautical Engineering, Kyoto University, Kyoto 606, Japan
‡ Aircraft Engineering Division, Kawasaki Heavy Industries Ltd, Kakamigahara 504, Japan

(Received 12 October 1987 and in revised form 17 September 1988)

Three-dimensional numerical calculations of an inviscid gas past scoops in a gas centrifuge are performed by solving the Euler equations using the explicit Roe upwind scheme with a second-order of accuracy. The scoop is modelled as a cylindrical or a wing-shaped rod attached to a central tube and extending radially outwards, and no inlet flow to the scoop is assumed. The scoops are placed close to the bottom end plate, and there is no covering baffle plate. The numerical grid employed is of the multibox type. The main results are as follows. For a cylindrical scoop, a detached bow shock is formed in front of the scoop. Behind the shock, strong radially inward motion of gas towards the central axis is induced, and it excites an upward flow which becomes a countercurrent. The inward flow just in front of the scoop produces a vortex column in the upstream region of the scoop. For a wing-shaped scoop, an oblique shock attached to the scoop is formed, and an inward flow is induced behind the shock. The shock is not so strong as that in the case of a cylindrical scoop model. The drag coefficient of the wing-shaped scoop is almost one-fourth of that of the cylindrical scoop. The addition theorem of the scoop drag is verified for the wing-shaped scoop.

1. Introduction

A gas centrifuge is a rapidly rotating long cylinder, in which a gas of isotope mixtures such as uranium are separated by the centrifugal force. In order to enhance separation, a counter-current flow is set up in the rotor by some means. In a thermally driven gas centrifuge, a countercurrent is induced by a temperature difference between the top and the bottom end plate or a temperature distribution on the sidewall.

A mechanically driven gas centrifuge utilizes scoops to generate a countercurrent. The scoop is a rod attached to a central feed tube, and it is fixed to the inertial frame and does not rotate with the cylindrical rotor. A rotating gas hitting the scoop loses angular momentum, and an inward motion of the gas, which generates the countercurrent, is induced. The scoop has another role: to collect either enriched or depleted gas (see figure 1).

It is almost impossible to measure a supersonic flow experimentally in a gas centrifuge, although there have been several works on subsonic flows. However, compressibility of the gas plays an essential role in a gas centrifuge. Therefore, we must rely on theoretical approaches to understand supersonic flows in a gas centrifuge.

The flow pattern of a thermally driven countercurrent has been analysed both

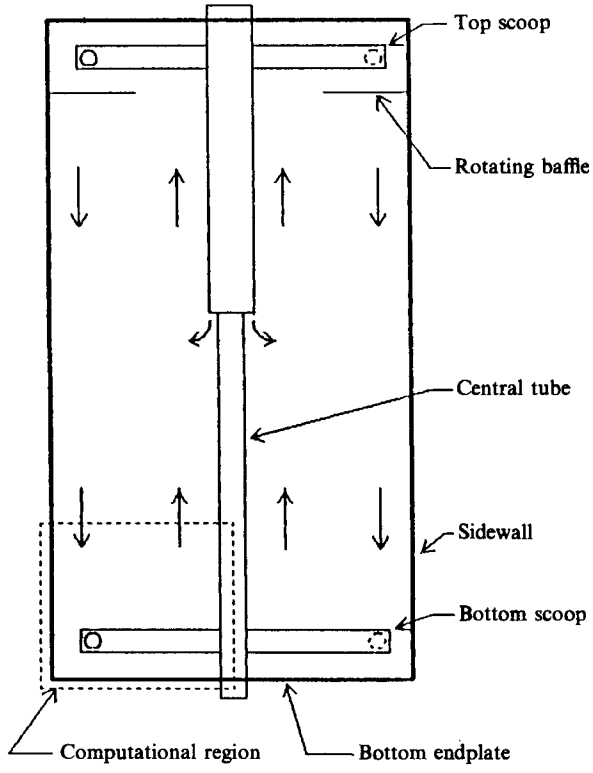

FIGURE 1. A schematic diagram of the flow field in a scoop-type (Zippe type) gas centrifuge. The region surrounded by the dashed line is considered in the present work.

analytically and numerically by many authors (Sakurai & Matsuda 1974; Nakayama & Usui 1974; Bark & Bark 1976; Wood & Morton 1980; see reviews by Olander 1972; Rätz 1978; Soubbaramayer 1979). The characteristics of a thermally driven countercurrent are well understood because of its relatively simple nature.

On the other hand, a flow induced by a scoop is essentially three-dimensional and nonlinear in nature, and the scoop flow is not yet well understood. In an analysis of the scoop flow, it has been customary to replace the scoop by an equivalent disk rotating slightly slower than the main rotor in order to make the problem a linearized axisymmetric one.

For example, Matsuda & Hashimoto (1976) assumed the angular speed of the equivalent disk to be $\Omega_0 - \Delta\Omega$. Although we could obtain the same countercurrent as the scoop-driven flow by assuming an appropriate form of $\Delta\Omega(r)$ of the equivalent disk, there are no theoretical grounds on which to choose this form.

Kai (1983*a*, *b*) computed the drag on the gas due to the scoop, and equated it with a viscous drag due to an axisymmetric equivalent disk. In his calculation, Kai assumed the drag coefficient C_d to be unity. In neither approach could a possible three-dimensional effect be taken into account, and so it is essential to know what is happening in the flow past scoops.

Sakurai (1981) analysed the scoop flow in terms of a linearized thin-wing theory, and verified the addition theorem of the drag due to the scoops, i.e. a scoop seems to be unaffected by upstream scoops (or itself, if only one scoop is present). Therefore, the drag is independent of the number of scoops.

On the other hand, T. Sakurai (1987, private communication) speculated a completely opposite picture for a blunt-nosed scoop. The wake behind a blunt-nosed scoop develops into a dead-air zone, in which the scoop is immersed. In this picture no shock waves are generated by the scoop. He speculated that Ekman layers develop between the dead air and the incident flow, and secondary flow is induced in the Ekman layers. The motivation of the present work is to find out if this picture is valid.

Hittinger, Holt & Subbaramayer (1981) and Hittinger *et al.* (1983) obtained a solution exhibiting a bow shock in front of a cylindrical scoop. Mikami (1981, 1985) performed two-dimensional numerical simulations of a flow about a scoop inlet, and Aoki & Suzuki (1985) computed three-dimensional inlet flows; they obtained shocks generated by the scoop. In these studies, however, they assumed a uniform upstream flow and considered only the region close to the scoop. The upstream effects of the scoops are completely neglected. In order to see if shocks are formed at all, three-dimensional calculations that include the whole region are essential.

Elsholz (1979), Volosciuk (1981), and Walz, Volosciuk & Schutz (1983) performed three-dimensional Navier–Stokes simulations of flows affected by a scoop. They modelled a scoop by a stationary disk extending in the azimuthal direction, although such a shape is not realistic. They obtained a secondary flow induced by the scoop, but shocks were not seen, probably because of the coarse mesh employed by them. A full Navier–Stokes calculation seems to be still premature considering the performance of the present day supercomputers.

The most relevant work for the present investigation is by Roberts (1985), who did N-body Monte Carlo simulations of gas impacting on a probe/scoop modelled as a cylindrical rod extending radially from the central axis. He showed large systematic motions induced in the gas by the obstacle, with strong radially inward-driven flow in the neighbourhood and downstream of the obstacle and a correspondingly large density perturbation in these regions.

Since Roberts used a Monte Carlo method, he could compute only the low-density central region of the centrifuge rotor. He also restricted his attention to the flow field near the scoop, neglecting the effect due to the upstream scoop.

In the present paper we shall give the first results of three-dimensional gasdynamic calculations of flows past scoops extending radially. Therefore, our work is to some extent complementary to that of Roberts: he considered an infinitely long cylindrical rotor, while we take into account the bottom end plate. We compute the whole flow region by assuming a periodic boundary condition, an assumption essential to settle the argument on the occurrence of shocks. We discuss two scoop shapes: cylindrical and wing-shaped.

We do not take into account the effect of viscosity explicitly in this work, and we solve Euler equations rather than the Navier–Stokes equations. Therefore, the Ekman layer and the Stewartson layer do not appear. Although the effect of viscosity is yet to be taken into account, this does not mean that it does not play any role in our calulation. In fact viscosity plays an important role in a thin shock layer in inducing a radially inward flow.

Since a centrifuge rotor rotates so rapidly that its central region is almost a vacuum, the fluid dynamical approach may be irrelevant. We truncate the central region by assuming a very thick solid inner tube, whose radius is assumed to be as large as $0.5R$–$0.7R$, R being the radius of the rotor.

We assume two, three or four scoops which are equally spaced in the azimuthal direction. Adopting a periodic boundary condition at an upstream and a downstream

boundary, there is always only one scoop in the computational region. The scoops are attached to the inner tube and extend radially up to $0.95R$. The radius of the cylindrical scoop and one-half of the thickness of the wing-shaped scoop are both fixed at $0.05R$. Their central axes are placed $0.1R$ above the bottom end plate. The half-vertex angles of the leading edge and the trailing edge of the wing-shaped scoop are 30°. There is no inlet section attached to the scoop, and no inlet flow is assumed. We are only interested in the secondary flow induced by the presence of the scoops. We place no baffle cover above the scoop in this work. The rotational Mach number is fixed at 7, so the peripheral speed is about 630 m/s.

In §2 the grid system and the numerical method of the flow calculation are explained. The results are presented in the §§3 and 4, and a conclusion and a discussion are given in the §5.

2. Numerical method

2.1. *Grid system*

Among various methods for generating a grid system, we adopt in the present study the multiblock transformation technique (Lee 1981; Rubbert & Lee 1982) combined with an algebraic grid generator because of its inherent geometrical flexibility to the wide class of complex three-dimensional geometries. An additional advantage of adopting the multiblock grid system is that a flow solver can be fully vectorized, retaining a longer vector length.

In the multiblock transformation, a body in the physical space is mapped on the surface of the corresponding hexahedral block in the computational space. The resultant grid has a similar structure as an *H-H-H* type grid system. In the course of surface/volume grid generation, we apply the transfinite interpolation method (Eriksson 1982). A complete description on our numerical methods can be found in Takanashi & Sawada (1987).

We have prepared several grid systems for the flow calculations. The standard grid for the cylindrical scoop (case 1 of table 1) has 50 azimuthal, 30 radial and 40 vertical grid points. The radius of the inner tube is set to 0.7 (normalized by the outer radius of the peripheral casing) while the length of the rotor is 0.3. The range of θ is from 0° to 180°, which corresponds to the case of two scoops. The other grid systems are listed in table 1. Figures 2(*a*) and 2(*b*) show a representative overall view of the grid systems of cases 1 and 6, respectively.

2.2. *Flow calculations*

We neglect the effect of viscosity in the present calculation so that the Euler equations written in the inertial frame of reference are solved. They can be written in vector form as

$$\boldsymbol{q}_t + \boldsymbol{E}_x + \boldsymbol{F}_y + \boldsymbol{G}_z = 0, \tag{2.1}$$

where

$$\boldsymbol{q} = \begin{pmatrix} \rho \\ \rho u \\ \rho v \\ \rho w \\ e \end{pmatrix}, \quad \boldsymbol{E} = \begin{pmatrix} \rho u \\ \rho u^2 + p \\ \rho uv \\ \rho uw \\ (e+p)\,u \end{pmatrix}, \quad \boldsymbol{F} = \begin{pmatrix} \rho v \\ \rho uv \\ \rho v^2 + p \\ \rho vw \\ (e+p)\,v \end{pmatrix}, \quad \boldsymbol{G} = \begin{pmatrix} \rho w \\ \rho uw \\ \rho vw \\ \rho w^2 + p \\ (e+p)\,w \end{pmatrix}, \tag{2.2}$$

Case	Grid			Range			M	Scoop
	I_{max}	J_{max}	K_{max}	r	θ	z		
1	50	30	40	0.7–1.0	0°–180°	0–0.3	7	cylinder
2	90	30	46	0.7–1.0	0°–180°	0–0.3	7	cylinder
3	50	40	40	0.5–1.0	0°–180°	0–0.3	7	cylinder
4	50	30	50	0.7–1.0	0°–180°	0–0.4	7	cylinder
5	50	30	40	0.7–1.0	0°–180°	0–0.3	3.5	cylinder
6	70	30	46	0.7–1.0	0°–180°	0–0.3	7	wing
7	70	30	46	0.7–1.0	30°–150°	0–0.3	7	wing
8	70	30	46	0.7–1.0	45°–135°	0–0.3	7	wing

TABLE 1. The grid systems used in the present calculations

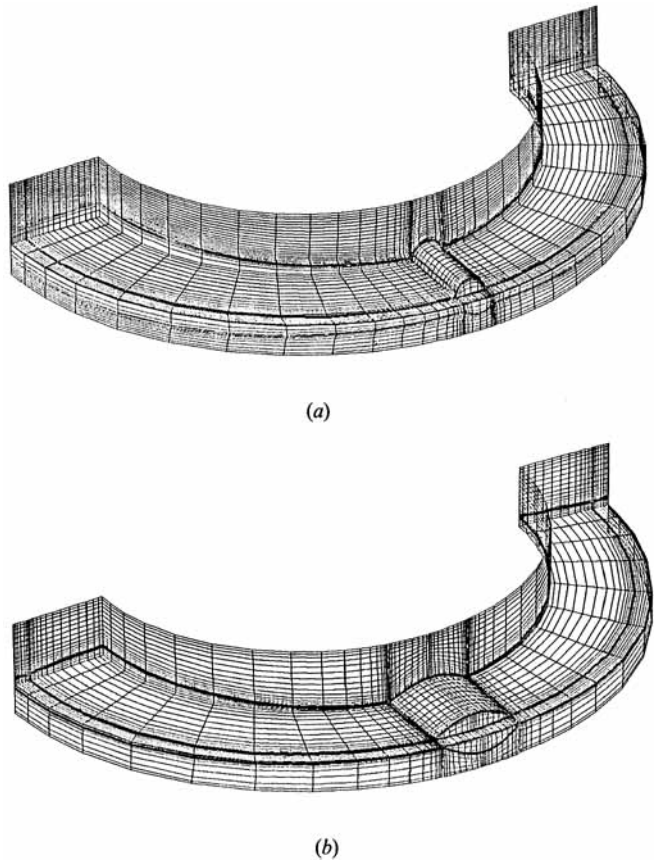

FIGURE 2. An overview of the computational domain and the grids for (*a*) the cylindrical scoop, and (*b*) the wing-shaped scoop.

where ρ represents the density, (u, v, w) are the Cartesian velocities, p the pressure and e the total energy per unit volume. The equation of state is given by

$$P = (\gamma - 1)\{e - \tfrac{1}{2}\rho(u^2 + v^2 + w^2)\}, \tag{2.3}$$

in which γ represents the specific heat ratio, which we fixed at 1.065 to simulate UF_6.

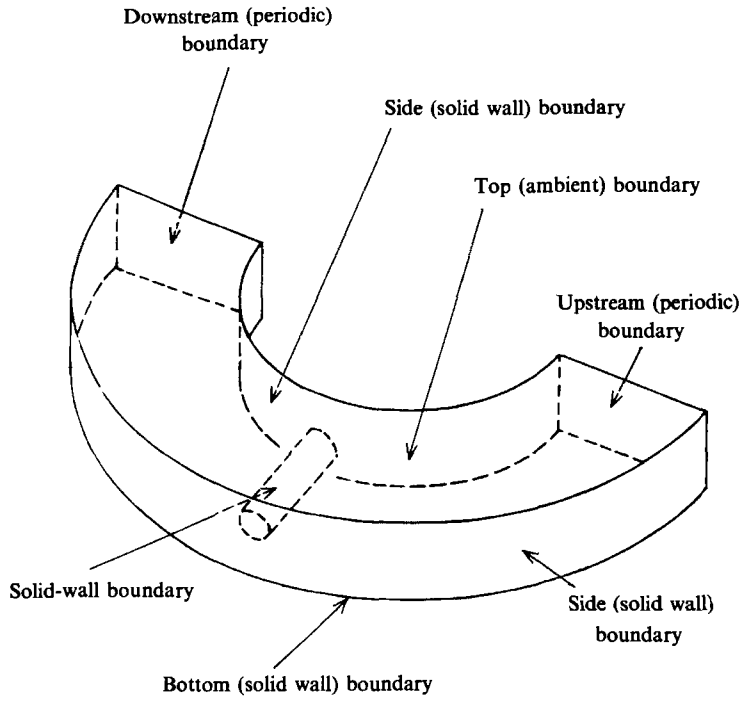

FIGURE 3. Boundary conditions.

The outer radius of the surrounding casing R is taken as the lengthscale. Velocities are normalized by the sound speed and density by its value at $r = R$ of an isothermal gas in rigid rotation with angular velocity Ω_0, which is the reference state of the present calculations. This state is also used as the ambient boundary condition, which will be described in §2.3.

We apply the upwind-baiased finite-volume method of the TVD scheme to (2.2). We follow the finite-volume formulation by Agrawal & Deese (1983), and define piccewise linear profiles of the conservative variables in each cell. To determine the numerical flux at the cell faces, we use Roe's approximate Riemann solver (Roe 1981). The integration of (2.2) in time is performed by a two-step explicit method. The accuracies in space and time are both second order. We use a local time-stepping method to accelerate the convergence. The notion of the TVD was introduced by Harten (1983) and has been advanced by many authors (see, for example, Chakravarthy 1986). A complete description of our numerical methods can be found in Sawada & Takanashi (1987).

2.3. *Boundary conditions*

The boundary conditions adopted in the present calculations are schematically illustrated in figure 3. The bottom wall and the sidewall of the casing as well as the surface of the scoop are treated as solid boundaries. Since we are solving the Euler equations, the mass flux and the energy flux vanish there and only the momentum fluxes due to the pressure force remain.

The upstream and downstream boundaries are treated as the periodic boundaries. On the top boundary, we apply the ambient boundary condition (Sawada *et al.* 1986) in which we assume fictitious cells located just outside the top boundary surface. The

physical quantities corresponding to an isothermal gas in rigid rotation are specified in these fictitious cells. The numerical flux at the top boundary is determined by solving the Riemann problem. Since we solve the Riemann problem by our upwind scheme, it does not require any additional work.

Since we solve the Euler equation written in the inertial frame of reference, there is no viscous force to drive the rotation of the flow, as in a real situation. The net torque to keep flows rotating in the calculation is supplied from the inflows, i.e. downdraughts, at the outer part of the top boundary. At the same time, possible shock waves penetrate, and outflows, i.e. updraughts, occur in the inner part of this boundary.

It should be stressed that we do not assume that the flow tends to that of rigid rotation with increasing z. We only assume that the gas in the peripheral region at large z rotates rigidly with the angular velocity Ω_0 because it is in the Stewartson layer in reality. The inflow only occurs at the outer part of the top boundary, and this inflow conveys the angular momentum of the rigidly rotating gas with $\Omega = \Omega_0$. In the inner region the updraught occurs, the vertical velocity component of which is subsonic. Therefore, only the characteristics of $w-c$, where c is a sound speed, enter from the top boundary into the computational region. Although the pressure of gas in the fictitious cells is felt by the gas in the computational domain, the rigidly rotating gas in the fictitious cell does not give a torque to the inner gas because of the upwind nature of our ambient boundary condition. Therefore, even if we extend our computational domain further in the axial direction, the computed angular speed would not approach that of rigid-body rotation. This expectation will be tested in our calculations.

The ambient boundary condition is a neat approach to realize an upwind and the non-reflecting nature. Inflows and outflows occur in quite natural ways according to the solution of the Riemann problem at the boundary surface. The influence of various numerical boundaries, including the present ones, on the simulation of laboratory free jet flows can be found in Matsuda *et al.* (1987).

3. Result for cylindrical scoops

3.1. *Test calculation*

The numerical methods described above have been applied to a test problem, i.e. supersonic flows past a sphere. The region covering a quarter-sphere is calculated, with $60 \times 30 \times 30$ grid points. The results were compared with a photograph in Van Dyke (1982) for Mach numbers of $M = 1.53$ and $M = 4.1$ and good agreement with the shock profiles was obtained.

3.2. *Standard case*

In this subsection we describe the result for case 1 in table 1. For the initial condition, we assumed a rigidly rotating gas in the computational region, and an impulsive start was applied. We monitored the inflow and the outflow of mass at the top boundary and also the drag coefficient, C_d, of the scoop to check the convergence. We found that all cases converged within a residue of less than 10^{-2} by 2000 steps. The CPU time is 1 h for 1000 steps by the Fujitsu VP200 vector processor and 47 min by the VP400 vector processor both at the Data Processing Center of Kyoto University.

Figures 4(*a*), 4(*b*) and 4(*c*) show the pressure contours in the (θ, z)-plane at $r = 0.94$, $r = 0.9$ and $r = 0.86$, respectively. At the tip of the scoop, a strong bow shock is seen, which becomes weaker as it travels inward.

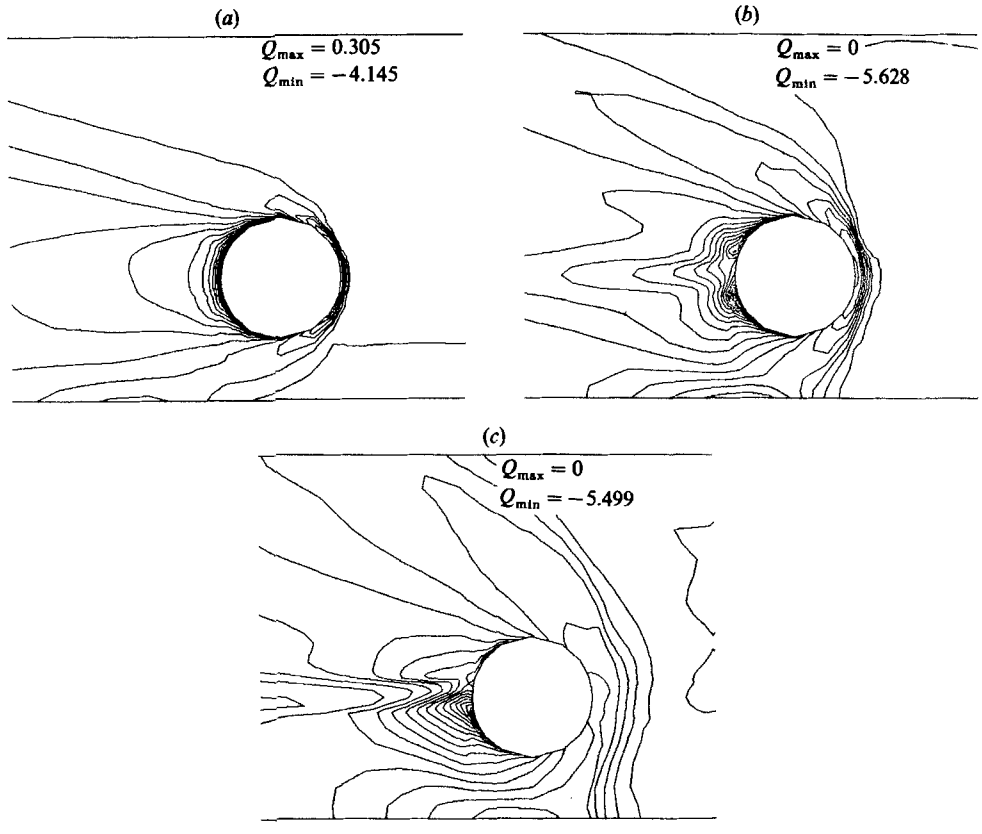

FIGURE 4. Pressure contours in the (θ, z)-plane at (a) $r = 0.94$, (b) $r = 0.9$, (c) $r = 0.86$. Q_{max} and Q_{min} show the maximum and the minimum contour lines of the logarithm of the dimensionless pressure, respectively, and the increment is 0.2.

Figure 5(a) shows the velocity vectors in the (r, θ)-plane at the scoop. Strong radially inward flow is seen in front of and behind the scoop. The inward flow ahead of the scoop reaches the inner solid boundary, and moves upstream to form a vortex. This vortex extends in the vertical direction and forms a vortex column. It was quite unexpected to find that the central region of a gas centrifuge rotates in the opposite direction from the rotor. As can be seen later, this phenomenon is common in the other cases with a cylindrical scoop, and, if correct, shows that a cylindrical scoop is not suitable from an engineering view point.

Figure 5(b) shows the pressure contours corresponding to figure 5(a). In the region near the scoop tip, the pressure stratification is considerably disturbed due to the shock.

Figures 6(a), 6(b) and 6(c) show the velocity vectors in the (r, z)-plane just in front of the scoop, at its centreline and just behind it, respectively. One can see the strong radially inward motion of gas, which hits the inner wall to form an updraught. Near the periphery the perturbations of velocities are almost invisible. Slight perturbations may cause large mass flows at the peripheral region because of the high density of gas.

Figure 7(a) shows the velocity contours of the vertical component of the flow (solid lines show the updraught and dotted lines the downdraught). This figure shows that there is a rather strong updraught in the central region of the rotor, and thus a

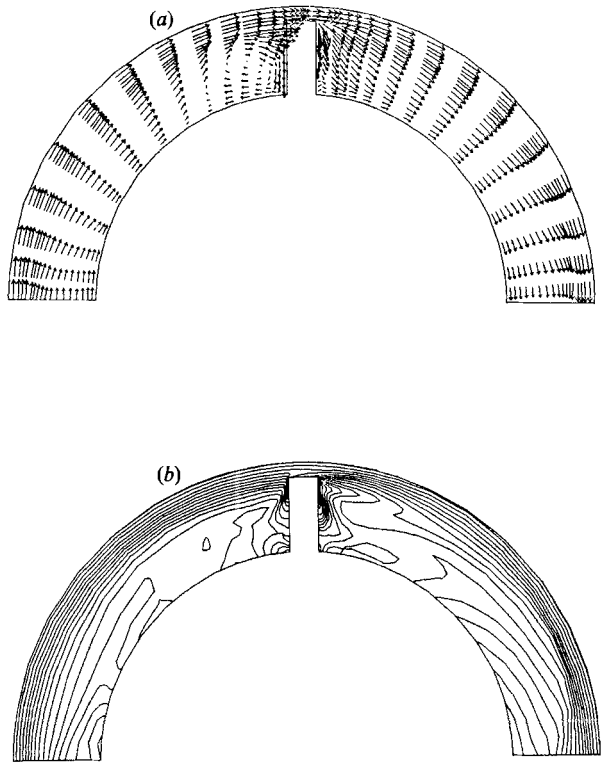

FIGURE 5. (*a*) Velocity vectors and (*b*) pressure contours in the (r, θ)-plane at the centreline of the scoop, $z = 0.1$. $Q_{\max} = 0.076$, $Q_{\min} = -4.682$, and the increment is 0.2.

countercurrent is produced. Figure 7(*b*), which shows the vertical mass flux at the top boundary, reveals that this countercurrent flow is restricted to very close to the peripheral region, because of the strong density stratification in the radial direction. We can also find a vertical wavy motion which produces downdraughts at $\theta = 0°$, 90° and 180° and updraughts at $\theta = 45°$ and 135°. We shall also see this phenomenon in the wing-shaped model.

Figure 8 shows the averaged vertical mass flux as a function of the radial coordinate. This figure shows that a countercurrent exists as a whole in spite of vertical wavy motion.

3.3. *The case with a smaller central tube*

What is the cause of the formation of the vortex column ahead of the scoop? The lack of viscosity in our model may permit the generation of the vortex column. If the inner tube is smaller, a vortex column may not be produced. Since taking into account viscosity is a future task, in the present study we investigate only the effect of the location of the inner wall.

The gas moving inward along the front face of the scoop collides with the central tube and turns upstream. To see this effect, we computed the case in which the inner boundary is placed at $r = 0.5$ instead of 0.7 (case 3).

We still observe the vortex column in front of the scoop. The counter-rotating region extended almost to the upstream boundary. Therefore, it is anticipated that

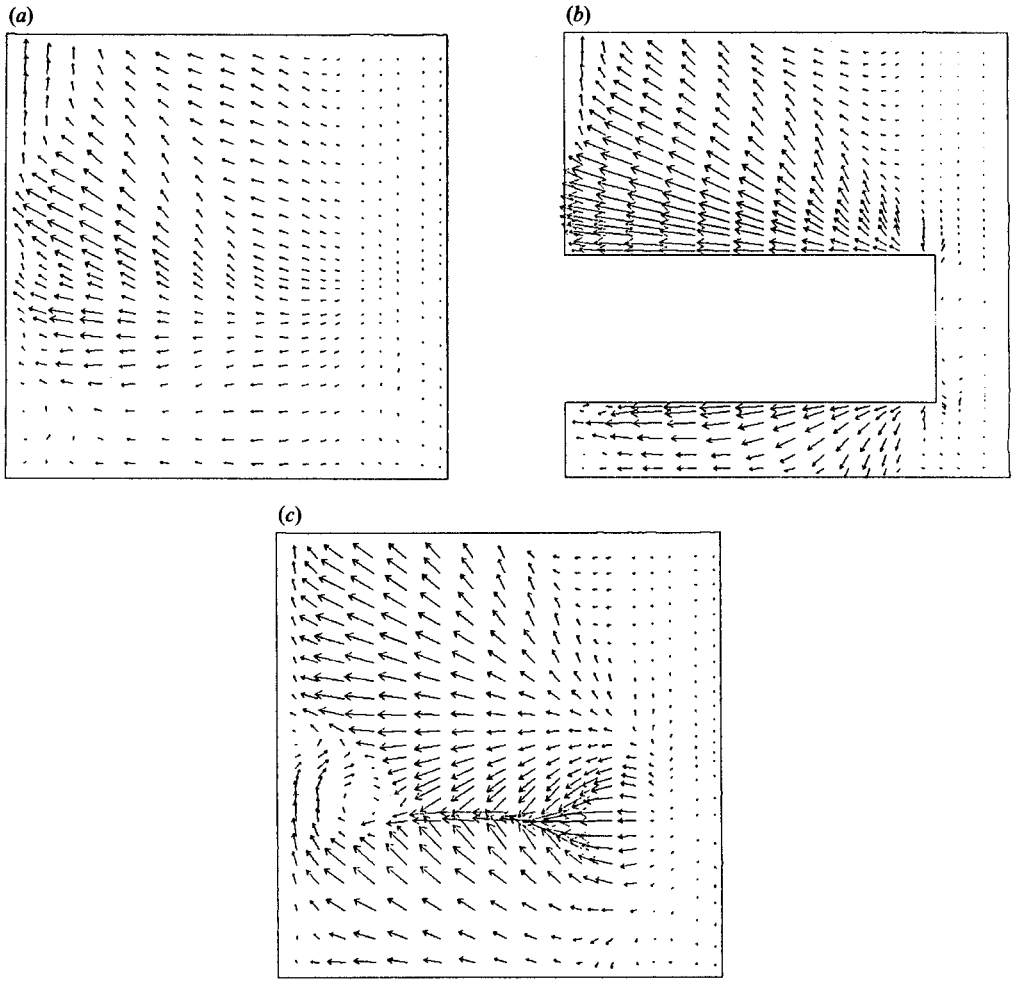

FIGURE 6. Velocity vectors in the (r, z)-plane, (a) just in front of, (b) at the centreline, (c) just behind the scoop.

the counter-rotating region will fill almost the entire inner core region, if the radius of the central tube is reduced further.

In figure 8 the dash-dot line shows the averaged mass flux for case 3.

3.4. *The case with a longer rotor*

In the previous case, the numerical top boundary conditions are applied at $z = 0.3$. In order to see the effect of the location of the boundary, we computed the case in which the top boundary is moved to $z = 0.4$ (case 4). In figure 8 a dashed line shows the averaged mass flux for case 4 at $z = 0.3$. It is almost the same as that for the standard case. Therefore, one can conclude that the rotor length of $z = 0.3$ is long enough for our purpose.

By comparing the three lines in figure 8, one can say that the choice of the boundary conditions does not have any significant effect on the countercurrent.

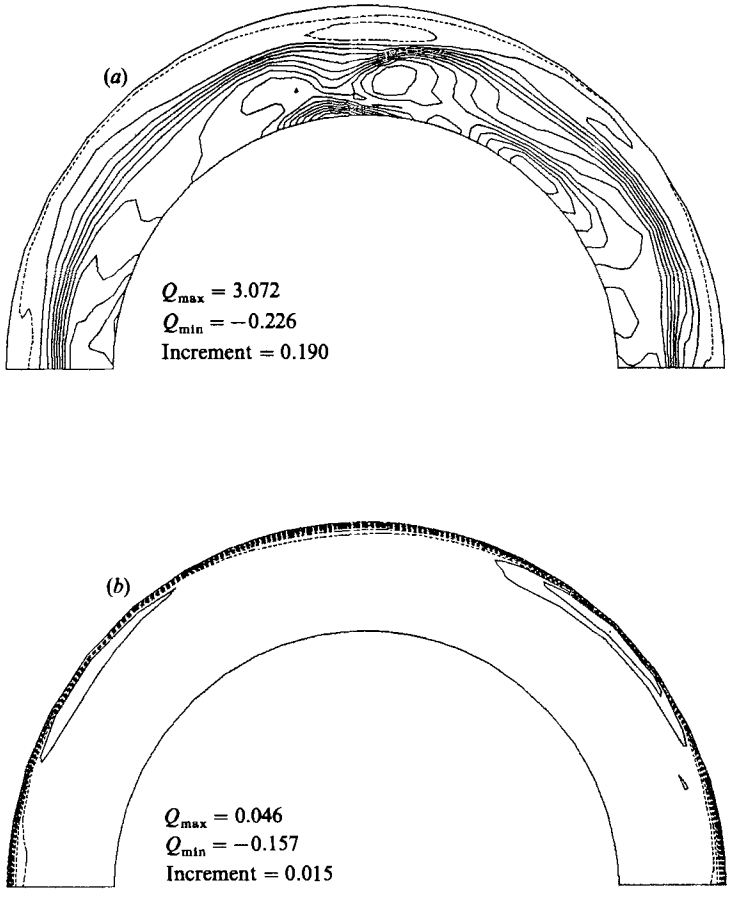

FIGURE 7. (*a*) Vertical velocity, w, in the (r, θ)-plane at the top boundary; (*b*) vertical mass flux, ρw, contours. Dotted lines show the downward flow.

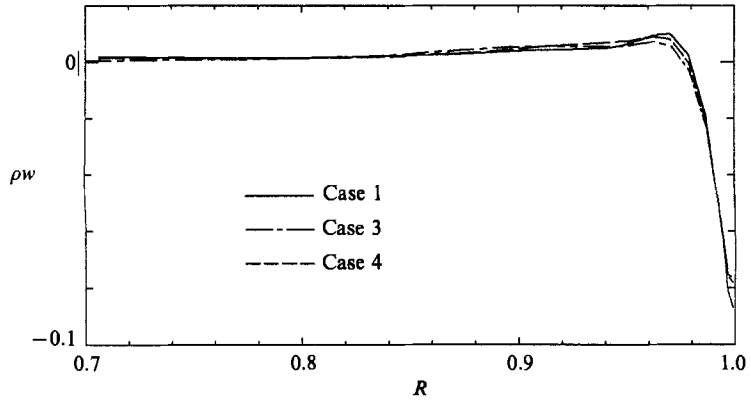

FIGURE 8. The vertical mass fluxes, ρw, averaged in the azimuthal direction for three cases: case 1 corresponds to the standard model, case 3 to the smaller central tube, and case 4 to the longer rotor.

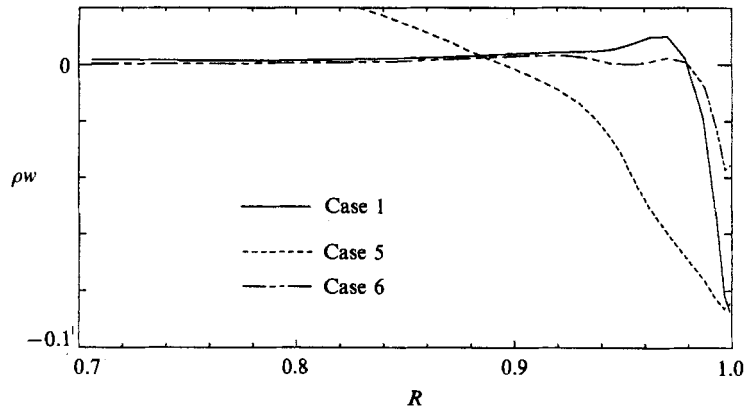

FIGURE 9. The vertical mass fluxes, ρw, averaged in the azimuthal direction for three cases: case 1 corresponds to the standard model, case 5 to a lower Mach number, and case 6 to a wing-shaped scoop.

3.5. *The case with a lower Mach number*

In all the above examples the Mach number at the periphery of the unperturbed gas was $M = 7$. In this subsection we examine the case in which $M = 3.5$ to see the effect of the peripheral velocity (case 5). We found that the radially inward motion in front of the scoop is weaker compared to the case at $M = 7$. However, we still observe a weak vortex column at the upstream side of the scoop. In figure 9 a dotted line shows the averaged mass flux for case 5. We can see that the peak of the updraught is shifted towards the central tube.

4. Results for a wing-shaped scoop

4.1. *Flow fields*

The real shape of the scoop of the gas centrifuge in the industrial use is classified, but in most theoretical works it is assumed to be a cylindrical rod for simplicity. In this subsection we investigate the case in which the scoops are wing-shaped bodies (case 6).

Figures 10(*a*), 10(*b*) and 10(*c*) show the pressure contours in the (θ, z)-plane at $r = 0.94$, $r = 0.9$ and $r = 0.84$ respectively. Strong attached oblique shocks are seen even at $r = 0.86$. Figure 11(*a*) shows the velocity vectors in the (r, θ)-plane at the scoop centre. In front of the scoop there is no inward flow and no vortex column is formed. One can conclude that the normal shock in front of the cylindrical scoop is responsible for the formation of the vortex column. Figure 11(*b*) shows the pressure contours.

Figures 12(*a*), 12(*b*) and 12(*c*) show the velocity vectors in the (r, z)-plane just in front of, at the centre and just behind the scoop, respectively. These figures show the inward flow behind the oblique shock. The deceleration by the oblique shock is weaker than for the cylindrical scoop and therefore the inward flow is weaker as well.

Figure 13(*a*) shows the velocity contours of the vertical component. It can be seen that a rather strong downdraught exists on the scoop. Just behind the scoop, there is a strong updraught, though these flows do not contribute as much to the vertical mass flux, as is shown in figure 13(*b*).

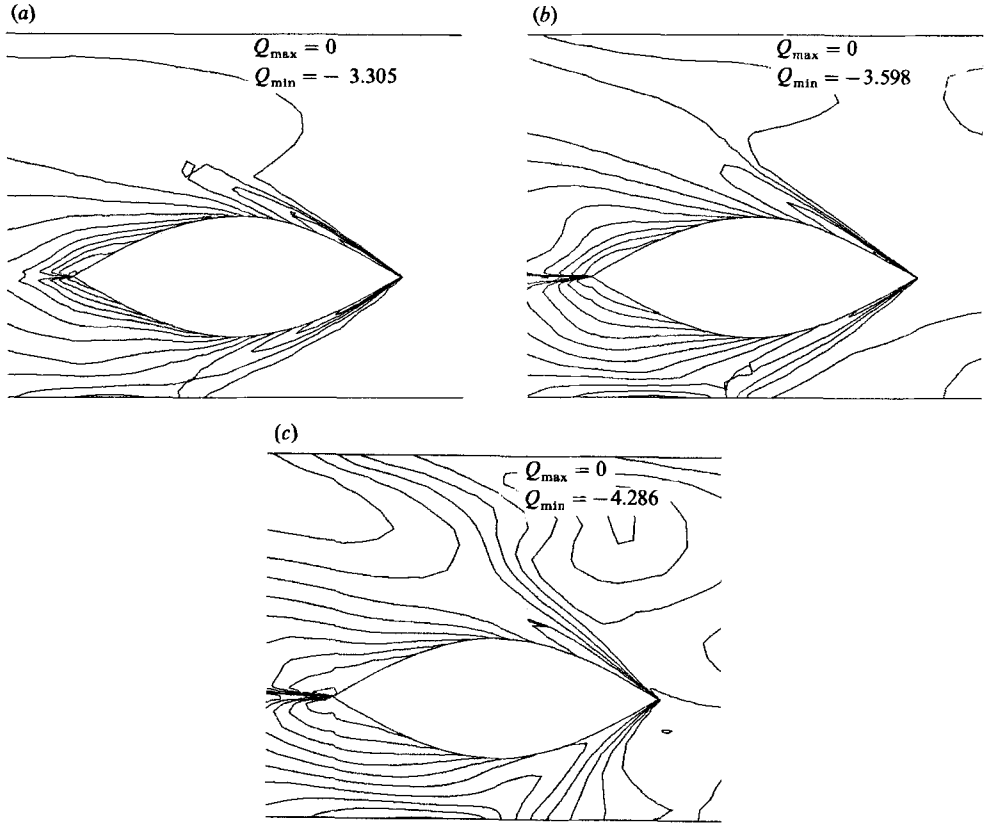

FIGURE 10. Pressure contours on wing-shaped scoops at (*a*) $r = 0.94$, (*b*) $r = 0.9$, (*c*) $r = 0.86$, and the increment is 0.2. One can observe strong attached shocks.

In figure 9 the dash-double-dotted line shows the averaged mass flux for case 6. We can see that the wing-shaped scoop produces a weaker countercurrent than the cylindrical scoop.

4.2. *The drag coefficient* C_d

In order to test Kai's assumption (Kai 1983*a*, *b*) that C_d is unity, the drag force is computed by integrating the θ-component of the pressure force acting on the scoop surface, and from it C_d is computed:

$$C_d = \frac{F}{\frac{1}{2}\rho v_\theta^2 D_s},$$

where F and D_s are the drag force and the thickness of the scoop. To normalize the density and the azimuthal velocity of gas, we used the unperturbed values rather than the computed ones.

Figure 14 shows the radial variation of C_d based on our model computed both by the coarse grid (case 1) and by the finer grid with cylindrical scoops embedded (case 2). They agree in general, and agree well at $r > 0.93$. This shows that our results based on the coarser grid are good enough for practical purposes, because the inner region does not contribute to the performance of the gas centrifuge very much.

We can also say that Kai's assumption is not too bad. At $r = 0.7$, however, C_d becomes as large as 70. This is inevitable since the density of gas in this region

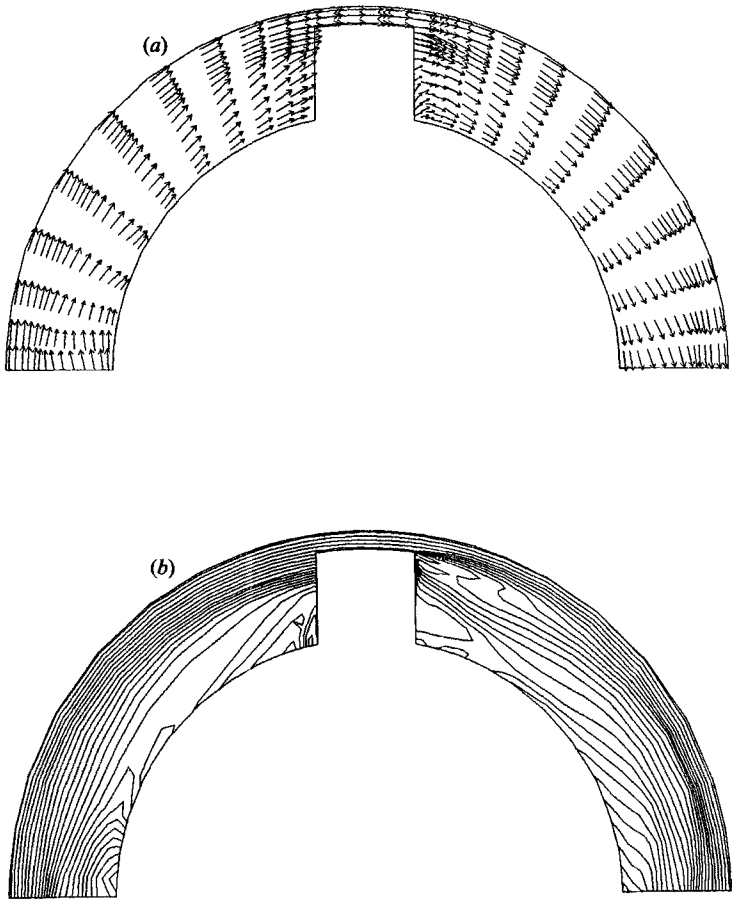

FIGURE 11. (a) Velocity vectors and (b) pressure contours in the (r, θ)-plane at the centre of the scoop, $z = 0.1$, for the wing-shaped scoop. $Q_{\max} = 0$, $Q_{\min} = -5.461$, and the increment is 0.2.

deviates very much from the unperturbed value, and the drag coefficient computed on the unperturbed quantity does not have any significant meaning there. However, the inner region is not very important.

Sakurai (1981) analysed the scoop flow in terms of linearized thin-wing theory and demonstrated the addition theorem for the scoop drag, i.e. the drag coefficients of scoops are independent of the number of scoops as long as the shock waves are attached to the scoop. We tested this theorem for wing-shaped scoops. We calculated C_d for three cases, in which the number of scoops N are 2, 3 (case 7) and 4 (case 8), respectively. Figure 15 shows the drag coefficient for these three cases. In the range $0.9 < r < 0.95$, C_d values agree well. Although Sakurai restricted his theorem to $r > 0.95$, our results suggests a wider range of applicability. It is considered that this theorem demonstrates the typical three-dimensional effect of a scoop flow. Although the existence of a scoop affects the flow field behind it, its effect is convected inward/upward by the countercurrent flow produced by the scoop. Fresh air rotating with angular velocity Ω_0 is supplied from the outer-upper corner, and the dead air is convected away. This is the reason why the addition theorem holds.

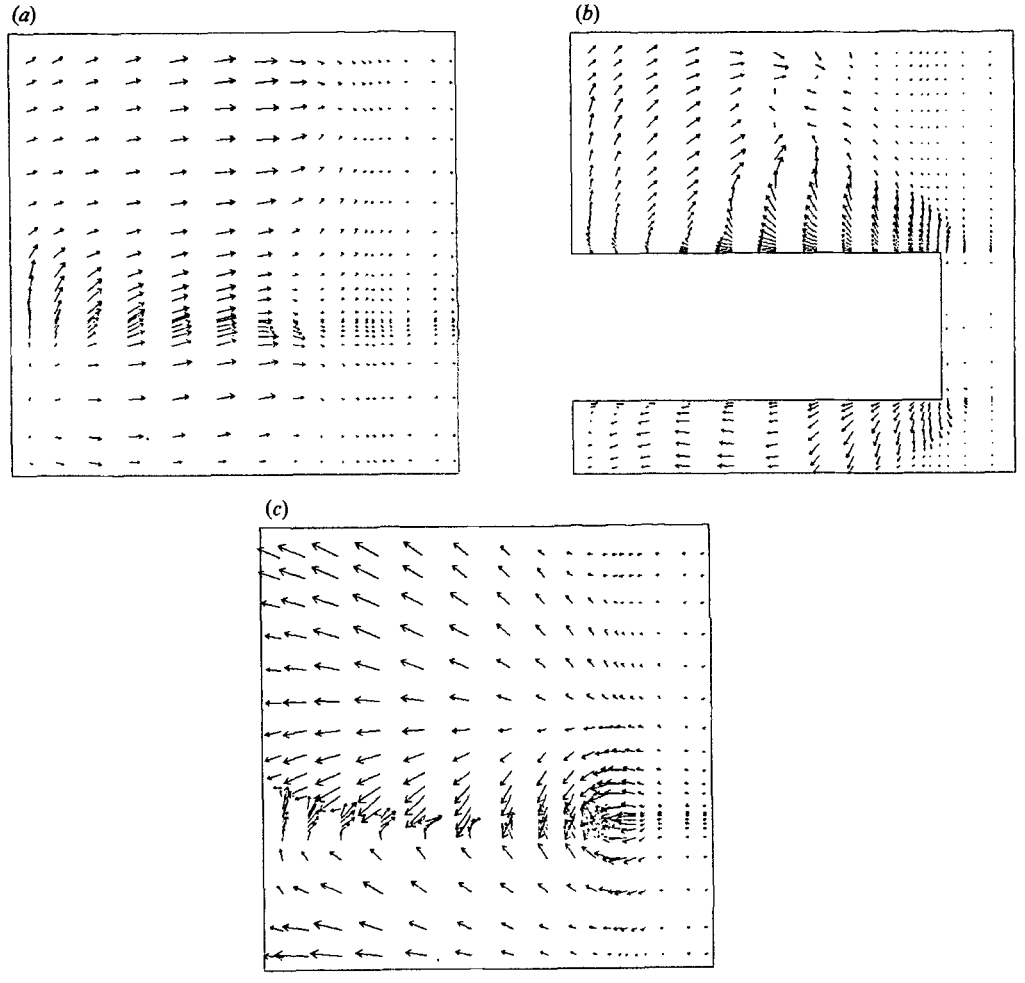

FIGURE 12. Velocity vectors in the (r, z)-plane, (a) just in front of, (b) at the centreline, and (c) just behind the scoop.

5. Conclusion and discussion

We have performed three-dimensional Eulerian calculations of flows past scoops in a gas centrifuge. Flow fields around two types of scoop, cylindrical and wing-shaped, were investigated for variety of cases. The algebraic method and the multiblock transformation technique were employed to generate grid systems. The Euler equations were solved by the second-order Roe upwind TVD method. We have obtained following results.

5.1. *Cylindrical scoops*

A strong bow shock was formed around the scoop tip, and the inward flow, which resulted in a countercurrent flow, was induced by it (see figures 4*a*, 5 *a* and 6). At the top boundary, the countercurrent was not uniform in the azimuthal direction but the averaged vertical mass flux showed the formation of the countercurrent as a whole (see figures 7*a*, *b* and 8). A vortex column is formed in front of the scoop. Therefore, the inner gas rotates in the opposite direction to the rotor (see figure 5*a*). By

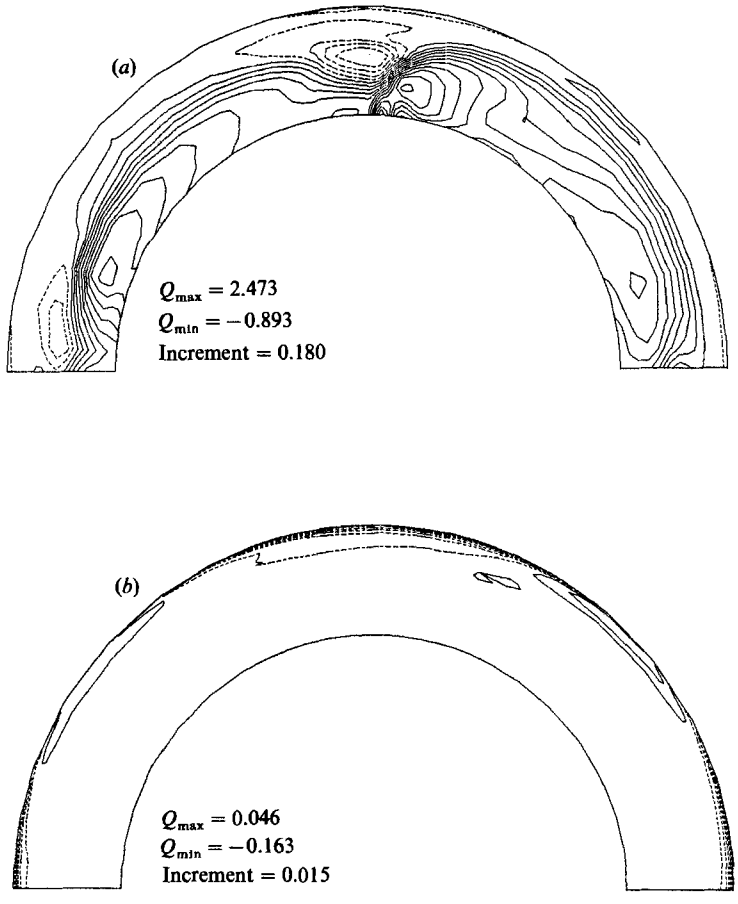

FIGURE 13. (a) Vertical velocity contours in the (r, θ)-plane at the top boundary; (b) vertical mass flux contours. Dotted lines show the downward flow.

comparing the three lines in figure 8, one can conclude that the choice of the boundary condition does not have any significant effect on the countercurrent.

5.2. *Wing-shaped scoops*

An oblique shock attached to the scoop was formed (see figure 10*a–c*). Behind the scoop an inward flow was induced (see figures 11 and 12*c*). It was not so strong as in the case of cylindrical scoops. There was no vortex column in front of the scoop (see figure 11*a*). The averaged mass flux was weaker, and the drag coefficient was almost one quarter of that for the cylindrical scoop. The addition theorem of scoop drag was verified (see figure 15).

5.3. *Discussion*

There are two major drawbacks to the present work: (*a*) the limited computational domain in the axial direction; (*b*) the neglect of viscosity. We discussed (*a*) in §2.3 on the boundary condition on the top numerical boundary, and pointed out that the rigidly rotating gas in the fictitious cell does not give a torque to the gas in the computational domain. However, this does not mean that the rigidly rotating gas does not have any effect on the gas in the computational domain. It may control the mass flux through the top boundary through the pressure balance. Therefore, the

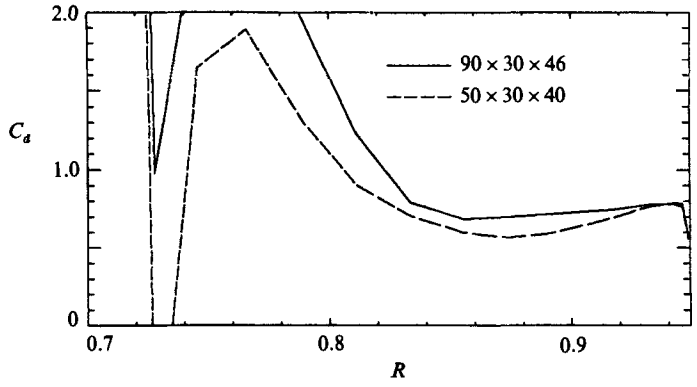

FIGURE 14. A comparison between the drag coefficient of a cylindrical scoop computed on the coarse grid (case 1) and on the fine grid (case 2).

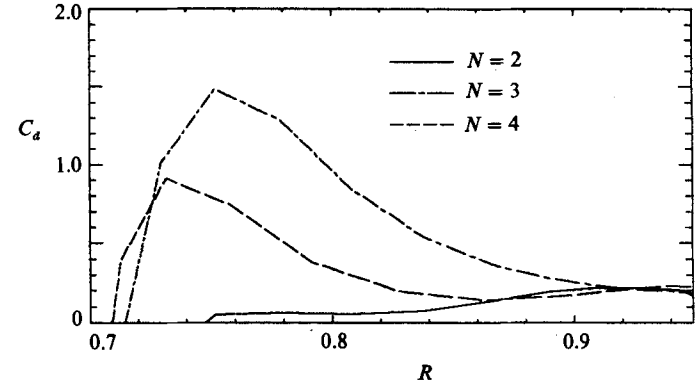

FIGURE 15. The drag coefficients in the presence of two, three and four wing-shaped scoops (cases 6, 7 and 8).

updraught velocity may be overestimated in our calculations. However, it is impossible to carry out inviscid calculations including the whole cylindrical region, because without viscosity there is no driving force to rotate gas.

The neglect of viscosity is certainly problematic. The picture of the complete flow field would be as follows. The bottom waste scoop decreases the angular momentum of the gas, and the fluid close to the scoop is pushed towards the rotor axis. The slowdown of the bulk of the fluid sets up Ekman layers both on the bottom end plate and on the baffle covering the top scoop. Meridional flows are set up which are closed through the outward radial motions in the Ekman layers and the vertical motions in the Stewartson layer.

Since we did not take into account viscosity, the bottom Ekman layer cannot exist, and therefore the outward radial motion of gas on the bottom end plate cannot be treated. The outward motion on the top baffle is implicitly assumed, though. Therefore, it may be argued that the differential rotation between the container and the bulk of the fluid, in our models, may not be large enough for the viscous forces in the Ekman layers to balance the drag on the bottom waste scoop. In realistic cases the slowdown of the bulk of the fluid may be so large that the strong shock at high Mach numbers would never occur. The ambient boundary condition may supply more angular momentum than the viscous forces could.

However, if such an argument is correct, the separation efficiency of the gas centrifuge would be much less than that calculated using conventional axisymmetric flow models based on an equivalent disk model (see for example Kai 1983*a*, *b*). Therefore, it would be plausible to assume that the bulk of the fluid rotates almost rigidly in reality. Moreover, it is natural to assume that the fluid in the downdraught through the outer part of the top numerical boundary has the angular velocity of the rotor, because such a downdraught should occur through the Stewartson layer, in which viscosity plays a dominant role in reality. In order to resolve this argument, however, we need to perform full three-dimensional Navier–Stokes calculations including the whole rotor.

The authors would like to thank Dr T. Kai for his valuable comments. We also thank an anonymous referee for his critical comments. The present calculations have been performed on the Fujitsu VP200/400 vector processors at the Data Processing Center of Kyoto University. This work was supported in part by the Grant-in-aid for scientific research (60302025) of the Ministry of Education, Science and Culture in Japan.

REFERENCES

AGRAWAL, R. K. & DEESE, J. E. 1983 Transonic wing-body calculations using Euler equations. *AIAA Paper* 83-0501.

AOKI, E. & SUZUKI, M. 1985 Numerical studies on gas flow around scoop of a gas centrifuge. In *Proc. Sixth Workshop on Gases in Strong Rotation, Tokyo* (ed. Y. Takashima), p. 11.

BARK, F. & BARK, T. 1976 On vertical boundary layers in a rapidly rotating gas. *J. Fluid Mech.* **78**, 749.

CHAKRAVARTHY, S. R. 1986 The versatility and reliability of Euler solvers based on high-accuracy TVD formulations. *AIAA Paper* 86-0243.

ELSHOLZ, E. 1979 Problems and successes in calculating axisymmetric and three-dimensional extraction chamber flow. In *Proc. Third Workshop on Gases in Strong Rotation* (ed. G. B. Scricini), Rome, p. 255.

ERIKSSON, L. E. 1982 Generation of boundary-conforming grids around wing-body configurations using transfinite interpolation. *AIAA J.* **20**, 1313.

HARTEN, A. 1983 High resolution schemes for hyperbolic conservation laws. *J. Comp. Phys.* **49**, 357.

HITTINGER, M., HOLT, M. & SOUBBARAMAYER, B. 1981 Numerical solution of the flow field near a gas centrifuge scoop. *Proc. Fourth Workshop on Gases in Strong Rotation, Oxford* (ed. E. Rätz), p. 22.

HITTINGER, M., HOLT, M., SOUBBARAMAYER & CORTET, C. 1983 Simulation of gas flow in front of the scoop of a gas centrifuge. In *Proc. Fifth Workshop on Gases in Strong Rotation, Charlottesville* (ed. H. G. Wood), p. 515.

KAI, T. 1983*a* Numerical analysis of flow of binary gas mixture with large mass difference in rotating cylinder. *J. Nucl. Sci. Tech.* **20**, 339.

KAI, T. 1983*b* Theoretical analysis of ternary UF6 gas isotope separation by centrifuge. *J. Nucl. Sci. Tech.* **20**, 491.

LEE, K. D. 1981 3-D transonic flow computations using grid systems with block structure. *AIAA Paper* 81-0988.

MATSUDA, T. & HASHIMOTO, K. 1976 Thermally, mechanically or externally driven flow in a gas centrifuge with insulated horizontal end plates. *J. Fluid Mech.* **78**, 337.

MATSUDA, T., UMEDA, Y., ISHII, R., YASUDA, A. & SAWADA, K. 1987 Numerical and experimental studies on choked underexpanded jets *AIAA Paper* 87-1378.

MIKAMI, H. 1981 Rotating supersonic flow about scoop inlet using an unsteady implicit technique. In *Proc. Fourth Workshop on Gases in Strong Rotation, Oxford* (ed. E. Rätz), p. 94.

MIKAMI, H. 1985 Two dimensional numerical calculation of flow fields about scoop inlet by the piecewise linear method. In *Proc. Sixth Workshop on Gases in Strong Rotation, Tokyo* (ed. Y. Takashima), p. 67.

NAKAYAMA, W. & USUI, S. 1974 Flow in a rotating cylinder of a gas centrifuge. *J. Nucl. Sci. Tech.* **11**, 242.

OLANDER, D. R. 1972 Technical basis of the gas centrifuge. *Adv. Nucl. Sci. Tech.* **6**, 105.

RÄTZ, E. 1978 Uranium isotope separation in the gas centrifuge. *VKI Lecture Series*. Von Karman Institute for Fluid Dynamics, Belgium.

ROBERTS, W. W. 1985 Three dimensional stratified gas flows past impact probes and scoops: N-body, Monte Carlo calculations. In *Proc. Sixth Workshop on Gases in Strong Rotation, Tokyo* (ed. Y. Takashima), p. 115.

ROE, P. L. 1981 Approximate Riemann solvers, parameter vectors, and difference schemes. *J. Comp. Phys.* **43**, 357.

RUBBERT, P. E. & LEE, K. D. 1982 Patched coordinate systems. In *Numerical Grid Generation* (ed. J. F. Thompson). North-Holland.

SAKURAI, T. 1981 Linearized thin-wing theory of gas-centrifuge scoops. *J. Fluid Mech.* **103**, 257.

SAKURAI, T. & MATSUDA, T. 1974 Gas dynamics of a centrifugal machine. *J. Fluid Mech.* **62**, 727.

SAWADA, K., SHIMA, E., MATSUDA, T. & INAGUCHI, T. 1986 The Osher upwind scheme and its application to cosmic gas dynamics. *Mem. Fac. Engng, Kyoto Univ.* vol. 48, No. 2.

SAWADA, K. & TAKANASHI, S. 1987 A numerical investigation on wing/nacelle interferences of USB configuration. *AIAA Paper* 87-0455.

SOUBBARAMAYER 1979 *Uranium Enrichment* (ed. S. Villani), p. 183. Springer.

TAKANASHI, S. & SAWADA, K. 1988 A generation procedure for 3D block structured grid systems. NAL *Tech. Rep.* to be published.

VAN DYKE, M. 1982 *An Album of Fluid Motion*. Parabolic.

VOLOSCIUK, K. 1981 Application of the vortex transport equations to the calculation of 2 and 3 dimensional extraction chamber flows. In *Proc. Fourth Workshop on Gases in Strong Rotation, Oxford* (ed. E. Rätz), p. 604.

WALZ, A., VOLOSCIUK, K. & SCHUTZ, H. 1983 Numerical investigations of the flow field near a model of a scoop using the vortex transport equations. In *Proc. Fifth Workshop on Gases in Strong Rotation, Charlottesville* (ed. H. G. Wood), p. 425.

WOOD, H. G. & MORTON, J. B. 1980 Onsager's pancake approximation for the fluid dynamics of a gas centrifuge. *J. Fluid Mech.* **101**, 1.